

# International Conference on Space Optics—ICSO 2018

Chania, Greece

9–12 October 2018

*Edited by Zoran Sodnik, Nikos Karafolas, and Bruno Cugny*



## *Optical communications downlink from a 1.5U Cubesat: OCSD program*

*T. Rose*

*D. Rowen*

*S. LaLumondiere*

*N. Werner*

*et al.*



icso proceedings



# Optical Communications Downlink from a 1.5U CubeSat: OCSD Program

T.S. Rose, D.W. Rowen, S. LaLumondiere, N.I. Werner, R. Linares, A. Faler, J. Wicker, C.M. Coffman, G.A. Maul, D.H. Chien, A. Utter, R.P. Welle, and S.W. Janson  
The Aerospace Corporation  
Mail Stop M2/246, P.O. Box 92957, Los Angeles, CA 90009-2957; 310.336.1157  
todd.s.rose@aero.org

## ABSTRACT

In this presentation, we discuss the first demonstration of a lasercom downlink from a LEO 1.5U 2.3 kg CubeSat to our optical ground station at The Aerospace Corporation in El Segundo, CA. Two vehicles, AC7-B&C, built under NASA's Optical Communications and Sensors Demonstration (OCSD) program and described in previous presentations, were launched in November 2017 and placed in a 450-km circular orbit. Following on-orbit checkouts and preliminary pointing calibration utilizing on-board star trackers, we have demonstrated (at the time of this manuscript submission) communications links up to 100 Mbps with bit error rates near  $10^{-6}$  without any forward error correction. Further optimization of the vehicle pointing and detection electronics and operating the transmitter at its full power capacity should enable performance improvements and potential for higher data rates.

## 1. INTRODUCTION

Small inexpensive satellite platforms offer opportunities for pathfinder experiments, space qualification of components and systems, and enhancement of larger assets. The Optical Communication and Sensor Demonstration (OCSD) is a two CubeSat flight test funded by NASA's Small Spacecraft Technology Program (SSTP) under the Space Technology Mission Directorate. Other SSTP efforts include ISARA, CPOD, PhoneSat and the eight-CubeSat Edison Demonstration of SmallSat Networks (EDSN) [1]. When initially proposed, the main objective for the OCSD mission was to demonstrate an optical downlink with a very modest threshold data rate of 5 Mbps, but subsequently set to 50 Mbps. As built, the AC-7B&C laser transmitters are capable of rates over 600 Mbps. Limitations in the scope of the OCSD program, however, set a top end rate goal of 200 Mbps. While 5.6 Gbps LEO satellite-to-ground links have been demonstrated from the NFire satellite to Tenerife [2] using high precision pointing, the present CubeSat architecture does not include an optical gimbal or any internal beam steering hardware. Eliminating the gimbal and moving parts reduces SWaP and cost, but requires setting the angular beam width to a milliradian or fraction thereof to accommodate a body pointed steering approach. This approach takes advantage of the exceptionally low moments-of-inertia of CubeSats, and their ability to perform rapid slew maneuvers. For pointing, we've developed miniaturized sun, Earth-nadir, and Earth-horizon sensors and cm-scale star trackers that provide the required attitude references for our attitude control system. Pointing accuracy and stability are key to any free space optical communications link. The overall trade-off is size, complexity and cost for communications bandwidth. While our experiments are not intended to demonstrate ultra-high bandwidth communications, the goal is to test the limits of technology that are enablers for low-cost rapidly-deployable small satellite platforms for optical communications, remote sensing and other applications. Further our strategy is to gain experience in manageable steps by setting reasonable goals and planning several low-cost missions to advance the state of the art.

## 2. OCSD FLIGHT/MISSION STATUS

The first OCSD, cataloged as "AeroCube-7A" (or AC-7A) was launched and deployed on Oct. 8, 2015. The optical communications hardware incorporated a two-stage Yb fiber master oscillator power amplifier (MOPA) system.

Initial on-orbit checkout proceeded as planned, until a software upload to the attitude control system (ACS) was interrupted by an unexpected spacecraft reboot. Subsequently the ACS was no longer functional and the laser subsystem was disabled. The follow-on OCSD mission utilizes two CubeSats (AC-7B&C) were launched on Nov. 13, 2017 aboard Orbital ATK's Cygnus resupply vehicle for NASA's ISS following an unexpected year and half delay post issues with the original host vehicles. The two AeroCube spacecraft, were deployed Dec. 06, 2017 occupy an orbit with a nominal height of 450 km and an inclination of 51.6 deg. Both CubeSats host a 2-4 W single-stage Yb fiber MOPA transmitter (detailed below) and silicon-based star trackers and mini reaction wheels constituting the critical hardware of the communications and pointing subsystems, respectively. At present on orbit pointing alignment has been completed with the C vehicle and is near completion with the B vehicle. Communication downlink tests to our ground station in El Segundo, CA are being conducted with AC-7B. Despite its incomplete pointing calibration (spiraling maneuvers are still being exercised), AC-7B offers a more intense downlink beam as described below. To date, transitory communication links at 50 and 100 Mbps have been demonstrated, with tests at 200 Mbps pending. Goals for proximity operations between the two AeroCubes, another major component of the OCSD mission and presented at this conference [paper SSC18-I-05], have successfully been completed.

### 3. SPACECRAFT HARDWARE AND PERFORMANCE GOALS

#### 3.1 The Spacecraft

As designed, the 1.5 U CubeSats weigh 2.3 kg and consumes ~2 W during most of the mission life. During lasercom engagements, which are expected to last ~3 minutes, the spacecraft will consume an additional 10-20 W power due depending on the set point of the laser transmitter. Operating with this thermal load even over a short period in a 1.5 U CubeSat is a thermal challenge. The laser system is mounted on an aluminum tray to transfer heat from the pump diodes, and this tray is thermally connected to the aluminum body. The body becomes a temporary heat sink and long-term thermal radiator. Unlike many commercial CubeSats, our exoskeleton, or "body", is machined from a single block of aluminum to provide structural and thermal stability. Figure 1, below, shows a breakout view of our AC-7B&C spacecraft.

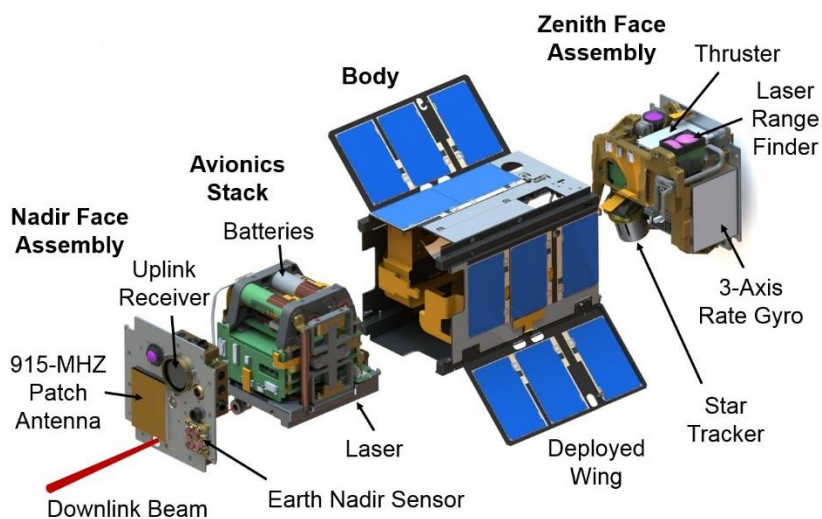


Fig. 1. Breakout of AC-7B&C spacecraft.

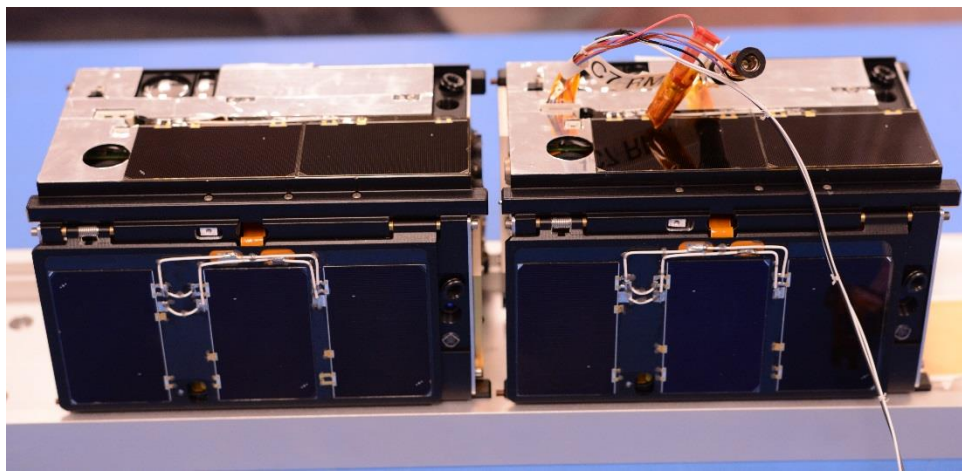


Fig. 2. Photo of AC-7B&C as delivered.

The wing surfaces and two of the rectangular side panels have three,  $\sim 1$ -W, triple-junction solar cells, while each of the remaining two rectangular side panels have two, 1-W triple-junction cells. Maximum solar input power is 9.5 W, and typical orbit-average power in 3-axis stabilized modes is 4.5 W. Two COTS 18650 size “high energy” lithium ion batteries with a total capacity of 14 W-hr provide spacecraft power during eclipse, and two COTS “high current” 18650 size lithium ion batteries provide over 15 W to the laser transmitter during optical downlinks.

### 3.2 Coarse Attitude Sensors

Since both spacecraft can and will fly with a wide range of orientations to support optical downlink and proximity operations, we incorporated six 2-axis sun sensors, four Earth-horizon sensors, a two-axis Earth-nadir sensor, and two sets of 3-axis magnetometers as basic attitude sensors. This combination of sensors allows continuous attitude determination with  $\sim 1^\circ$  accuracy even with multiple attitude sensor failures. The coarse attitude sensors provide an initial estimate of spacecraft attitude that is sent to the star tracker system for “fine” attitude control.

Our sun and Earth nadir sensors, described in previous work, have successfully flown on three different spacecraft missions. [3, 4] Once calibrated, our sun sensors have a  $0.32^\circ$  root mean square (rms) error, over a  $\pm 35^\circ$  field-of-view, in two axes. Based on flight data from multiple missions, our Earth nadir sensor has  $1^\circ$  accuracy in two axes. Errors typically result from using COTS optical temperature sensors that see thermal radiation from 5 to 14 microns in wavelength. Parts of this band can see all the way to the ground while other parts only see high altitude clouds that are typically cold.

Each spacecraft has four COTS Melexis MLX90620 infrared array sensors as an attitude-determination experiment to locate the Earth’s warm limb against cold space. These sensors have a  $4 \times 16$  array of thermopile temperature sensors that can optically read temperature with a 0.25 K (rms) temperature difference from  $-50^\circ\text{C}$  to  $300^\circ\text{C}$  at a 4 Hz rate. [5] Each pixel has a  $3.75^\circ \times 3.75^\circ$  FOV, potentially enabling nadir determination accuracy of  $\sim 0.3^\circ$  when all four sensors can see the Earth’s limb. These sensors provide a backup to the legacy Earth nadir sensor and should be less affected by cold, high-altitude clouds.

### 3.3 Fine Attitude Sensors and Pointing

As a primary approach, precision pointing of about  $0.024^\circ$  is achieved using star trackers. A secondary approach that is available (for comparison), but not activated to date, implements an uplink ground laser beacon (5W at 1550 nm) and onboard quad cell for closed-loop pointing. Both methods are expected to provide better than  $0.015^\circ$  attitude knowledge, while heritage 3-axis reaction wheels will provide a  $0.015^\circ$  control authority. This level of pointing accuracy is significantly better than the  $\sim 1^\circ$  pointing accuracy provided by our previous attitude sensors [6].

Error Sources	Pointing Error 3 $\sigma$ (Deg)
<b>Payload to AD Frame Alignment (post-cal)</b>	0.010
<b>Real-time Clock Drift</b>	0.005
<b>Orbit Determination / Ephemeris Error</b>	0.003
<b>Attitude Determination Error</b>	0.015
<b>Attitude Control Error</b>	0.015
<b>Total</b>	<b>0.024</b>

The dual star trackers on each CubeSat use an On Semiconductor MT9V022 monochrome WVGA imager coupled to f/1.2 lenses. A Spartan-6 FPGA reads an image frame, processes the field, and outputs a collection of star locations. These data are further processed by a 16-bit microcontroller using a star catalog to output pointing direction as a set of quaternions. One of the star trackers points 20° off the +Z direction (typically zenith), while the other is canted by 70° to provide angular diversity in case stray light from the moon, sun, etc. interferes with one tracker. Star fields are imaged about once every 1.5 seconds, and quaternion outputs are combined with more rapid rate gyro data to provide continuous attitude information with less than 0.1° error.

For robustness and power control, we have two 3-axis rate gyros on each spacecraft. A Sensoror STIM-210 3-axis rate gyro provides a bias stability of 0.5°/(hour)<sup>1/2</sup>, but it has a maximum power consumption of 1.5 W and needs a one-hour warm-up period. [7] These devices are susceptible to helium exposure that can occur during launch vehicle preparations, so we mount them inside their own hermetically-sealed container. We discovered this issue on AeroCube-4 using the legacy STIM-202.

Another set of rate gyros is in the VectorNav VN-100 inertial measurement unit (IMU), also on each spacecraft. [8] These gyros provide a bias stability ~10°/(hour)<sup>1/2</sup>, but the IMU consumes only 0.33 W. This IMU also contains a 3-axis set of accelerometers, a 3-axis set of magnetometers, and a pressure sensor.

### 3.4 Attitude Actuators

Attitude actuators include a triad of magnetic torque rods and a triad of reaction wheels. Our torque rods have a magnetic moment of 0.2-A-m<sup>2</sup>. They provide torques for detumbling and reaction wheel unloading. Our reaction wheels have flight heritage on multiple spacecraft with 1-mN-m-s of total angular momentum. Slew rates can be in excess of 5° per second using these wheels, and pointing control to within 0.015° has been demonstrated on-orbit using these reaction wheels on a similar spacecraft. Additionally, the CubeSats can slew about a single axis at rates of up to 20°/s, but are not anticipated to exceed 1.5°/s.

### 3.5 On board ACS data

In a typical laser pointing at the ground station scenario, maximum slew rates are on the order of 1.0 degrees per second. During the time intervals shown in Figures 3 and 4, the satellite was rotating faster than 0.5 degrees per second to support the laser pointing to the ground station. Given the star tracker solution consists of more stars than the minimum number required to obtain an attitude solution, the relative geometry of the detected star centroids can be compared against the star catalog positions to derive residual errors. The root mean square (RMS) of these residual errors can provide a rough estimate of the star tracker solution uncertainty (Figure 3).

The attitude control error computed in Figure 4 is a comparison of the commanded pointing trajectory with respect to the measured attitude (based on a blending of star tracker and rate gyro measurements). Many of the transients observed in the attitude error are the result of new star tracker updates being blended into the attitude determination solution. Given the star tracker solution uncertainty estimated from the star matching residual errors, the magnitude of these transients is somewhat expected. The overall laser pointing error is dominated by the star tracker solution uncertainty. Higher accuracy star trackers have been developed for follow-on missions which should further refine the body steered laser pointing accuracy. Independent observations of the laser signal at the ground station during spiral scan patterns are generally consistent the estimated pointing accuracy derived from the satellite telemetry.

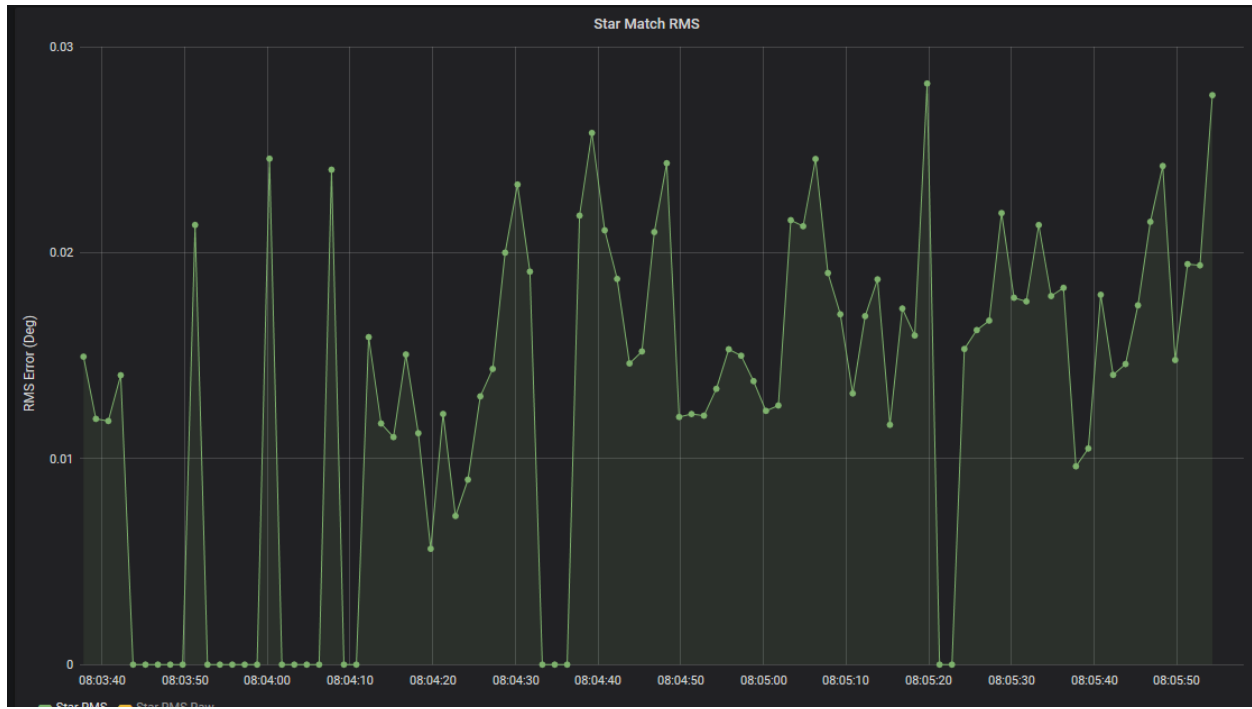


Fig. 3: Root Mean Square (RMS) errors of Star locations w.r.t. catalog geometry for four to eight matched stars. Note time intervals with fewer than four stars matched are mapped to zero RMS error on this plot.

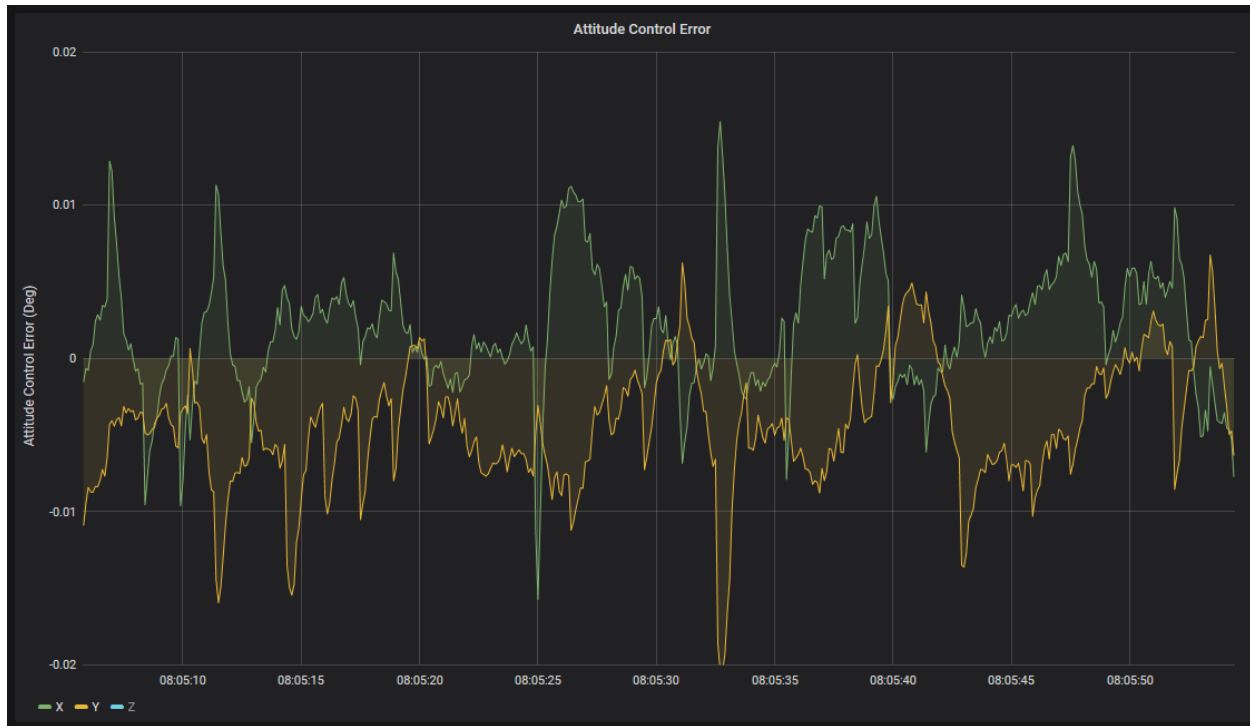


Fig. 4: Attitude Control Error Telemetry during laser downlink. Note that the laser is nominally aligned with the Z axis on the OCSD vehicles, so only the angle error about the X and Y axes influence the laser pointing and are shown for clarity.

## 4. THE OPTICAL DOWNLINK

### 4.1 The Laser Transmitter

Data encoding (OOK) is achieved by modulating the current of a low power DFB (master oscillator). The encoded optical signal is amplified from  $\sim 10$  mW to 2-4 W by a single stage polarization-maintaining ytterbium-doped fiber amplifier. Figure 5 shows a schematic of the transmitter, which is composed of COTS parts and designed to operate over a temperature range of 10-50 °C. Due to power constraints, the only element that is actively cooled is the laser diode master oscillator in order to control the output wavelength. The Yb fiber is pumped at 915 nm rather than at 975 nm to accommodate the large expected temperature range on orbit. Although pumping at 975 nm would have been more efficient and required less gain fiber, wavelength stabilized pump modules at 975 nm were found to have much poorer performance than unlocked devices at 915 nm and they were not able to stay locked over the entire temperature range. As designed, the AC7 transmit lasers are capable of delivering a max optical power of 4 W at 1064 nm with a wallplug efficiency of 20%. Just prior to delivery of the CubeSats for integration with the launch vehicle, however, a rework of the 7B laser system became necessary, which resulted in a reduced max output power around 3 W. For the initial on-orbit lasercom tests (discussed here), both transmitters are running at 2 W. Because of the uncertainty in the performance of the attitude control system (ACS) in this first time demonstration, the divergences of the output beams for 7B and 7C were set conservatively to be  $\sim 0.06$  and  $0.15^\circ$  FWHM, respectively. The 7B divergence is roughly twice the believed pointing accuracy ( $0.024^\circ$ , as described above) that could be realized from the ACS.

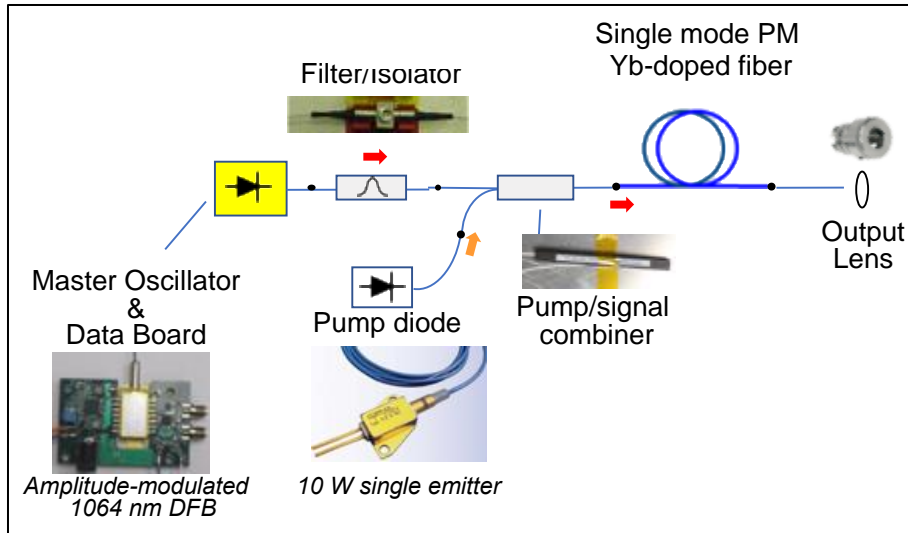


Fig. 5. Schematic drawing of the laser downlink transmitter.

Figure 6 shows photos of the laser transmitter slice (during assembly) that occupies a volume of  $\sim 10 \times 10 \times 2.5$  cm. The components are mounted to an aluminum baseplate with fiber windings on both sides. Nusil and heat conducting epoxy are used to dissipate the heat that is generated in the laser diode pumps and the gain fiber (not shown in the figure), respectively. A small lens (shown in fig. 6c), placed after the amplifier stage, is adjusted to yield the desired output divergence.

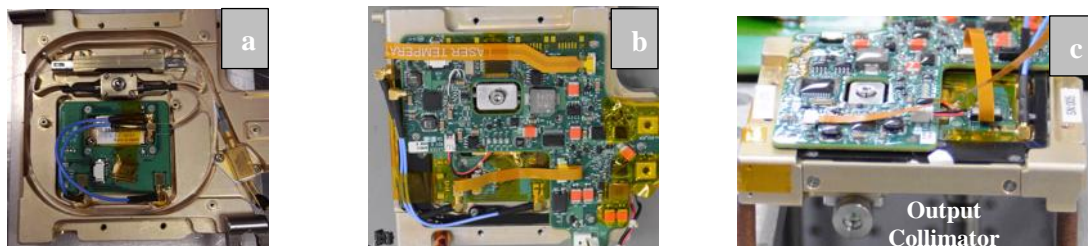


Fig. 6: Photos of the laser transmitter slice during build: (a) initial layout of components, (b) integration of laser control electronics and (c) output lens visible on underside, which also holds the fiber amplifier.

#### 4.2 Optical Ground Station & Receiver

The ground terminal consists of a 40-cm 3 m fl Ritchey–Chrétien telescope (shown in Figure 7) that is mounted on a conventional az-el gimbal arrangement and is controlled by in-house developed software. This software also links to two Xenics InGaAs camera arrays that can be used for active tracking. One of the cameras shares a common path with a high-speed APD detector; both are mounted on the back end of the telescope. In the current configuration, a beam splitter is used to split off 10% of the incoming light to the tracking camera, which provides a  $0.10^\circ \times 0.12^\circ$  field of view (FOV) whereas 90% of the light is sent to a high-speed large area Si-APD detector. The second InGaAs camera is mounted on the side of the main telescope and provides a  $1.5^\circ \times 1.8^\circ$  FOV.

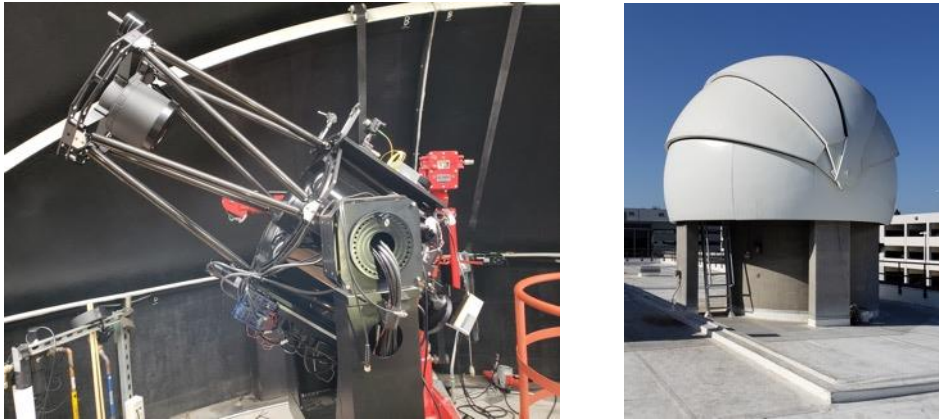


Fig.7: 40 cm optical telescope and ground station dome.

The Si-APD receiver converts the optical signal into an electrical one which is decoded by an in-house built modem. The modem performs clock and data recovery and for PRBS patterns that are transmitted by the spacecraft, logs bit errors and bit error rates (BERs). For the initial experiments at 50 and 100 Mbps the FOV of the APD is and sufficiently large, 0.057°, that only open loop tracking is required. Trajectory files are generated from on-board GPS data that is telemetered to one of several RF ground stations prior to the optical engagement. As smaller detectors are implemented for increased data bandwidths, closed loop tracking will be implemented if required.

### 4.3 CubeSat Space-to-Ground Pointing

Accurate pointing of the spacecraft is critical for the optical downlink to be successful and is dependent upon the accuracy of the star trackers and knowledge of the alignment between the star trackers and the laser. Initial tests to characterize the alignment involve successive spiral sweep patterns of the Cubesat about the projected location of the ground terminal. Time stamped received signal strengths recorded with the tracking cameras on the ground are analyzed with the satellite attitude determination data from the onboard star trackers and rate gyros to derive the relative alignment between the laser and the star tracker reference frame. As knowledge of the pointing is increased, the spiral pattern angular spread is reduced. An example of a 1° scan is shown in Figure 8. Note that the evaluation of the received signals strengths to optimize alignment must take the link range into account, which is constantly changing during the engagement. Further, repeat scan measurements are needed to account for non-systematic atmospheric losses due to clouds.

AC7-B Ground Station Illumination Progression: 5-17-2018

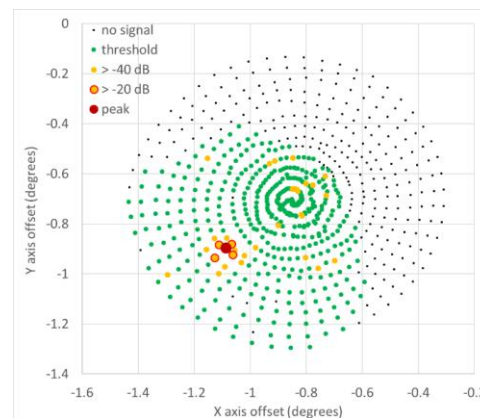
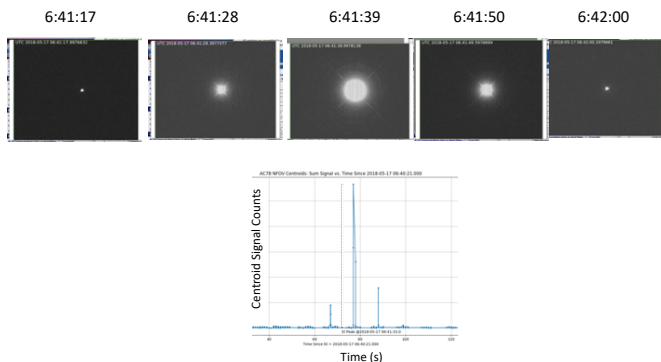


Fig. 8: Example results of a  $1^\circ$  spiral scan taken during the early phase of the AC-7B alignment. The image sequence on the left show five successive “hits” on the NFOV camera that are spaced roughly 11 seconds apart which corresponds to the angular scan rate of the spiral. The relative magnitudes of the hits are shown in the plot below. The plot on the right shows the calculated scan pattern (from the telemetry) on the ground (light blue dots) and positions of hits on the detector (green, orange and red dots) with the strongest hit denoted by the large red dot. Note that the center of this scan was offset by  $\sim 0.8^\circ$  based on prior scan results.

#### 4.4 Optical Downlink Performance: First Results

Optical engagements with the satellite are approximately 3 minutes long and are presently limited to elevation angles between  $30^\circ$  and  $70^\circ$ . (The laser is turned on only when the elevation angles are  $\geq 30^\circ$  and the telescope is purposely limited to angles below  $70^\circ$  as a precaution.) A data/BER collect at 50 Mbps (PRBS23) is shown in Figure 9 where the bit errors were recorded over 100 ms intervals. As shown in the figure, BERs near  $1E-6$  and below were observed with numerous intervals being error free (set to  $1E-9$  for convenience). Figure 10 shows results captured at 100 Mbps. During this scan we observed BERs approaching  $1E-6$ , but did not see any error free intervals. Note at the time of both collects, the Cubesat was exercising a scan pattern since we have not completed the final alignment. Hence, downlink data was not observable for the entire engagement and appears periodic. Link budget estimates indicate that lower BERs should be achievable and we will continue to assess the link performance as the system is optimized.

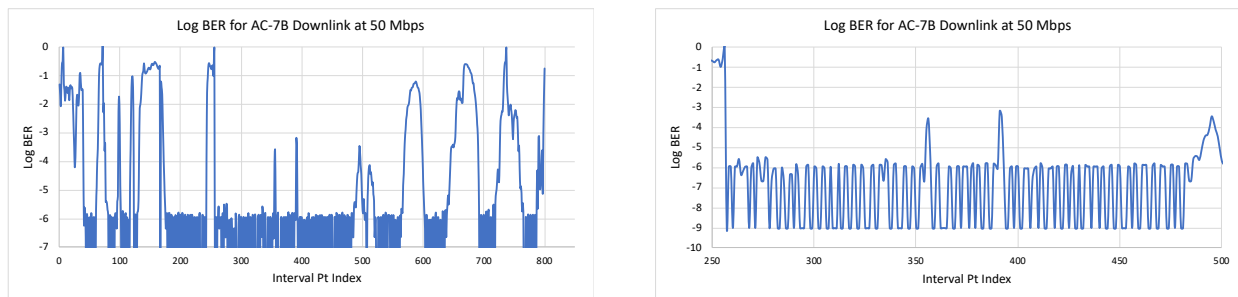


Fig. 9: BER collects at 50 Mbps over  $\sim 100$  ms intervals (rt); expanded view of a segment of the scan (lft).

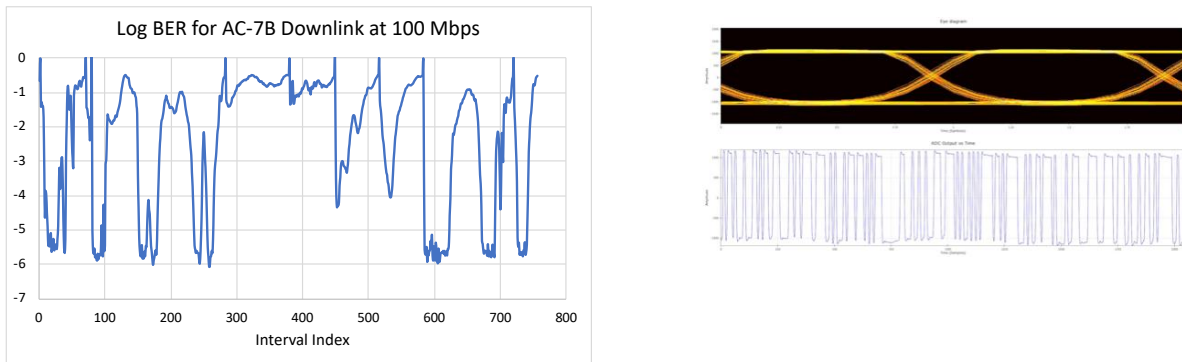


Fig. 10: BER collects at 100 Mbps over 100 ms intervals. The figure on the right is a snapshot of the waveforms sampled by the modem.

## 5. SUMMARY

The NASA OCS D program is a flight validation mission to test commercial-off-the-shelf components and subsystems that will enable new communications and proximity operations capabilities for CubeSats and other small spacecraft. Following the loss of the first CubeSat, AC-7A, the recent demonstrations with the two follow-on vehicles, AC-7B&C, have clearly satisfied the lasercom and proximity mission objectives and have exceeded all baseline goals.

For the communications portion of the mission, which is the topic of this submission, 50 and 100 Mbps LEO-to-ground links were demonstrated using our ground terminal in El Segundo which is near sea level. At the time of this submission, the links were performed under non-ideal conditions with pointing and receiver optimization still in progress. Under these conditions we achieved BERs near  $1E-6$  without any FEC. Link budget estimates indicate that lower BERs should be achievable and we will continue to assess the link performance as the system is optimized. Further we demonstrated sufficient vehicle pointing accuracy with on-board star trackers to close the links, as opposed to using an uplink beacon. The alignment corrected pointing accuracy of the CubeSat appears to agree (or may even exceed) the calculated values. Open loop pointing of the ground station was found to be adequate for the data rates achieved so far.

*All trademarks, service marks, and trade names are the property of their respective owners.*

## References

- [1] H. Smith, S. Hu, and J. Cockrell, "NASA's EDSN Aims to Overcome the Operational Challenges of CubeSat Constellations and Demonstrate an Economical Swarm of 8 CubeSats Useful for Space Science Investigations," paper SSC-XI-2, AIAA/USU Small Satellite Conference, Logan, Utah, Aug. 10-15, 2013.
- [2] R. Fields, D. Kozlowski, H. Yura, R. Wong, J. Wicker, C. Lunde, M. Gregory, B. Wandernoth, and F. Heine, "5.625 Gbps Bidirectional Laser Communications Measurements Between the NFIRE Satellite and an Optical Ground Station," Proc. of the 2011 Int. Conf. on Space Optical Systems and Applications, pp.44-53, Santa Monica, CA, 11-13 May 2011.
- [3] S.W. Janson, B. S. Hardy, A.Y. Chin, D.L. Rumsey, D.A. Ehrlich, and D.A. Hinkley, "Attitude Control on the PicoSatellite Solar Cell Testbed-2," paper SSC12-II-1, 26th Annual AIAA/USU Conference on Small Satellites, Logan, Utah, Aug. 2011.
- [4] S.W. Janson and D.J. Barnhart, "The Next Little Thing: Femtosatellites," paper SSC13-VI-3, 27th Annual AIAA/USU Conference on Small Satellites, Logan, Utah, Aug. 2013.
- [5] Melexis Microelectronic Systems, MLX90620 datasheet, URL: <http://www.melexis.com/Assets/Datasheet-IR-thermometer-16X4-sensor-array-MLX90620-6099.aspx>, Melexis Microelectronic Systems, Ieper, Belgium, May 2013.
- [6] S. W. Janson and R.P Welle, "The NASA Optical Communication and Sensor Demonstration Program: An Update," paper SSC14-VI-1, 28th Annual AIAA/USU Conference on Small satellites, Logan, Utah, Aug. 2014.
- [7] Sensoror AS, Butterfly Gyro STIM210 Multi-Axis Gyro Module datasheet, URL: <http://www.sensoror.com/media/90317/datasheet%20stim210%20ts1545.r10.pdf>, Sensoror AS, Horton, Norway, May 2013.
- [8] VectorNav Technologies, VN-100 web page, URL: <http://www.vectornav.com/products/vn100-smt>, VectorNav Technologies, Dallas, TX, 2014.

### **Acknowledgements**

The authors wish to thank R. Dolphus, J. Wilson, P. Carian, B. Hardy, D. Hinkley and A. Berman of The Aerospace Corporation for their contributions to this effort. The authors also wish to thank the NASA Small Spacecraft Technology Program for funding this work and the NASA AMES POC, R. Hunter.